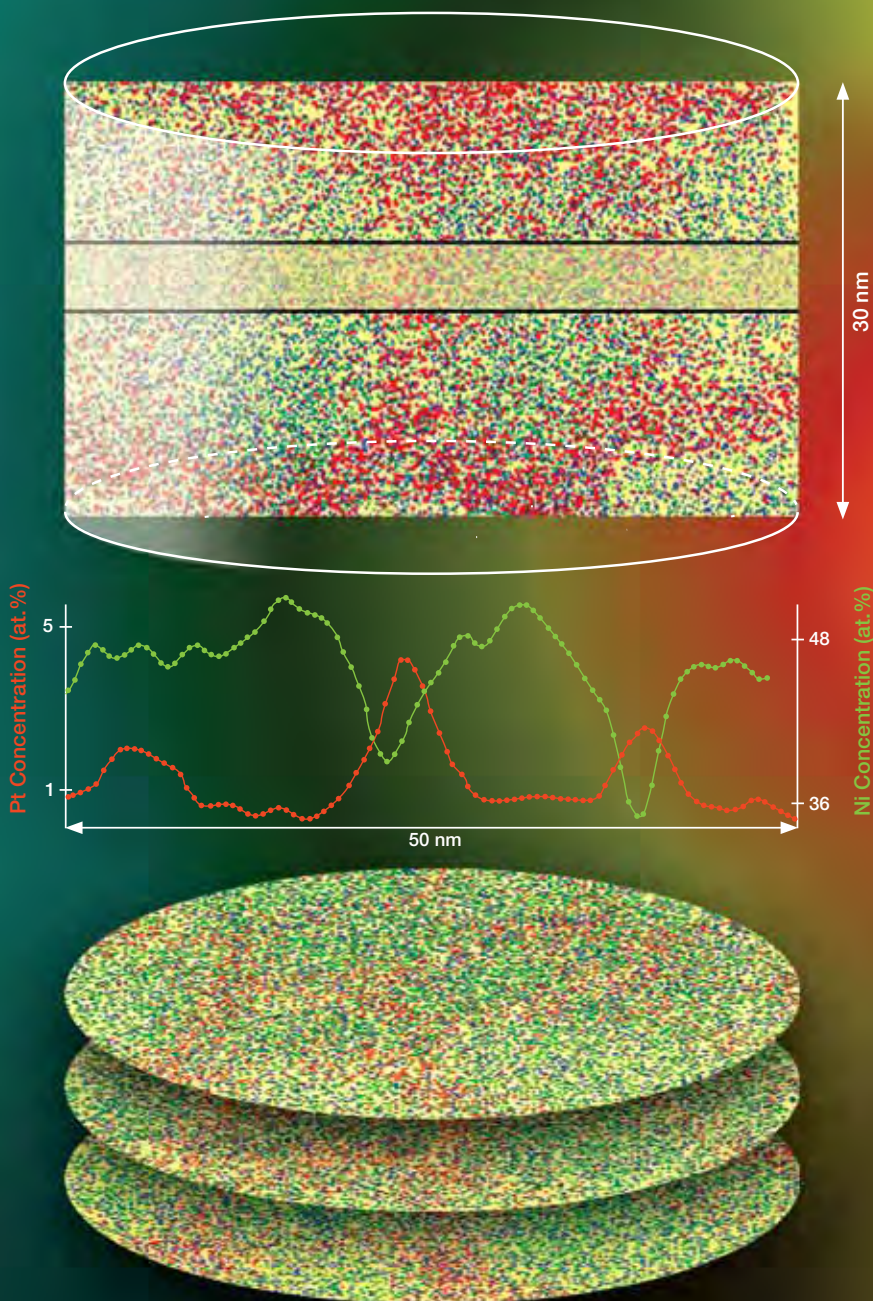


A Renaissance in Atom-Probe Tomography



Prospects for Nanobiology with Atom-Probe Tomography

Thomas F. Kelly, Osamu Nishikawa,
J.A. Panitz, and Ty J. Prosa

Abstract

The merits of atom-probe tomography (APT) of inorganic materials are well established, as described in this volume. However, one of the long-held aspirations of atom-probe scientists, structural and chemical characterization of organic and biological materials at near-atomic resolution, has yet to be fully realized. A few proof-of-concept type investigations have shown that APT of organic materials is feasible, but a number of challenges still exist with regard to specimen preparation and conversion of raw time-of-flight mass spectrometry data into a three-dimensional map of ions containing structural and chemical information at an acceptable resolution. Recent research aided by hardware improvements and specimen preparation advances has made some progress toward this goal. This article reviews the historical developments in this field, presents some recent results, and considers what life science researchers might expect from this technology.

Introduction

Materials of all types are being studied and developed at the atomic scale. Materials scientists have a long history of processing materials to obtain new structures and then characterizing these structures as a way to understand both the processing and the properties. Similar approaches are being applied to organic and biological materials (i.e., nanobiology), whether they are synthetically processed or naturally processed.

An essential element of any such endeavor is characterization capabilities. Materials science researchers have had microscopies for imaging and analysis at the atomic scale for decades, including transmission electron microscopy (TEM), x-ray diffraction (XRD)/crystallography, secondary ion mass spectroscopy (SIMS), and scanning probe microscopies (SPMs). These techniques do not, however, always offer the same full set of benefits for organic materials. For example, radiation damage and other beam effects in organic

materials limit the spatial resolution achieved in TEM to 1 to 2 nm, whereas 0.1 nm is possible in inorganic materials. XRD offers high spatial resolution atomic structure under the special circumstances of a crystallized specimen and large volume ($\sim 10^{-2}$ mm³) that limit its applicability to a small fraction of biological structures of interest (e.g., less than 15% of technologically important proteins).

Thus, the prospect of compositional imaging of biological materials at the atomic scale and in three spatial dimensions would seem to be self-evidently important to achieve. Atom-probe tomography (APT) has the potential to reach this goal, while offering several important advantages for organics analysis. The minimum sample size could be very small (zeptoliters). The time to data and time to knowledge can be short (days). The specimen material could be extracted from a native, likely frozen, environment (see discussion of cryogenic methods later in

this article) without the need for concentration, crystallization, or staining. Three-dimensional (3D) compositional mapping may be obtained from complex structures with high specificity on location. The spatial resolution of the data could be better than 0.5 nm. As a mass spectrometry-based technique, APT has high sensitivity (≈ 10 atomic parts per million) and high detector efficiency ($\approx 50\%$) for all elements in the periodic table and molecular components.

This is a powerful list of performance specifications that would surely have an important impact on imaging and analysis of organic and biological materials. But can it really be achieved? This article explores this question, presents some historical background for the work, and concludes that useful results from APT of organics is likely, although exactly how good remains to be demonstrated.

Molecular Imaging in High Electric Fields

The field-electron-emission microscope (FEEM) and the field-ion microscope (FIM) provide a simple and elegant way to observe a metal surface in near atomic resolution. In these devices, electrons or ions are projected almost radially from a sharply curved surface of radius, R , to an imaging detector a distance, D , from the surface. The projection magnification, $M \approx D/R$, for a given radius can be changed by varying D . Magnification is achieved without the aberrations of a lens system, and these microscopes are immune to vibration because of the typically high projection magnification.

For many years, attempts were made to use the FEEM to image organic molecules by Müller¹⁻³ and Melmed and Müller.⁴ These attempts were inspired by the simplicity of the technique and the potential for achieving high image contrast, magnification, and resolution. By 1950, the FEEM had demonstrated a usable magnification of 10^6 and an image resolution better than 2 nm. As a result, there was growing optimism that individual molecules might eventually be imaged. Although striking images displaying the correct symmetry of individual flaventrene and copper-phthalocyanine molecules were observed, it soon became apparent that identical FEEM patterns were produced by many different molecules.⁵⁻⁷ It is not known why these molecules were chosen for this work, but it may be because these molecules are planar, so they do not perturb the local field much, and they can be sublimed in vacuum. Several theories were advanced to explain the field-emission patterns.⁸⁻¹¹

Maps of the field-emission tunneling barrier subsequently confirmed that individual flaventrene and copper-phthalocyanine molecules had not been observed,¹² but rather, the patterns display the symmetry of electron emission from the molecule's density of states in these high-field surface conditions.

The low-temperature FIM provided another opportunity for examining molecular structure, but with greatly improved image resolution (0.2 nm under optimum conditions).^{13,14} However, the high electric field strength, E , required for field-ion imaging ($\approx 20 \text{ V nm}^{-1}$) proved to be a major obstacle. The problem is exacerbated if large biological molecules are deposited on a surface.¹⁵ Such molecules behave as large, weakly bound protrusions that can experience an outwardly directed, electrostatic field stress, $\sigma_d = e_0 E^2 / 2$, that translates into a pressure of about $1.8 \times 10^9 \text{ Pa}$ ($2.6 \times 10^5 \text{ psi}$), which can distort, destroy, or even remove a molecule from a surface; e_0 is the permittivity in free space.

To shield a molecule from the effects of the imaging field, ingenious schemes have been developed for embedding deposited molecules within a metallic matrix and imaging as the matrix was exposed by field evaporation.^{16–18} Unfortunately, image contrast in the pseudomorphic transition layer that contained the molecules prevented them from being recognized.

Imaging in the FEEM also was problematic because only transient images could be recorded with a movie camera at the earliest stages of image formation.¹⁹ The results were not convincing, although a double-blind protocol was used to identify the images. Most images did not reflect the known structure of the molecules, and few were reproducible.

The imaging attempts were constrained by an inability to confirm that biological molecules had been deposited on the surface. Subsequent protocols were developed using electron microscopy to confirm the deposition.^{20–22} As a result of these protocols, the 10-cm atom probe was used to develop a nondestructive, tomographic reconstruction procedure.^{23–28} This was obtained as a blanket of vitreous benzene ice that was field-desorbed from the surface. Resolution is limited to $\approx 1 \text{ nm}$ by the size of the benzene molecule (Figure 1).

Three-Dimensional Imaging with Atom-Probe Tomography

The application of APT to the study of biomolecular structure has been at the proof-of-principle stage since the advent of pulsed-voltage APT,^{30,31} but during the past

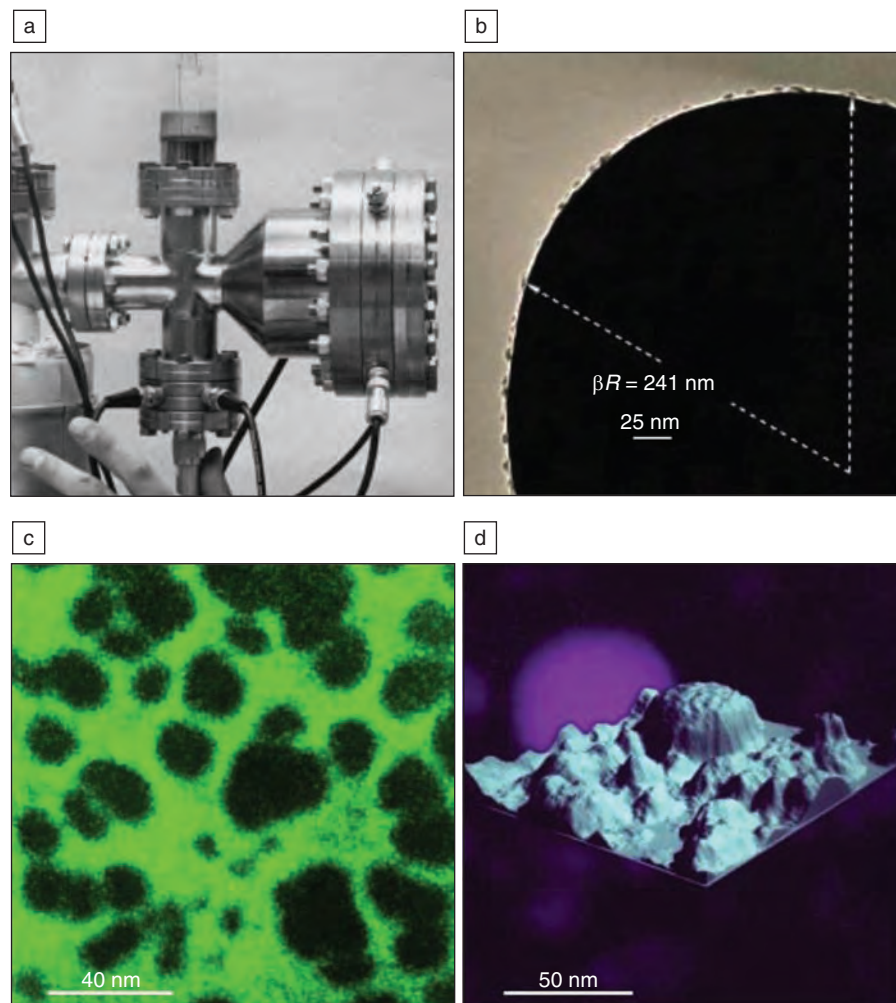


Figure 1. (a) A 10-cm atom probe. (b) A ferritin monolayer on tungsten (where $\beta \approx 1.5$ is the image compression factor, and R is the apex radius of the tip). (c) A contour slice image of a ferritin monolayer. (d) A tomographic reconstruction of a ferritin monolayer embedded in vitreous benzene ice.²⁹ Reprinted with permission from Cambridge University Press. ©2005, Microscopy Society of America.

five years, an increased availability of pulsed-laser APT (PLAP) has initiated a rebirth in these efforts.^{32–39} The introductory article by Seidman and Stiller provides an overview of how FIM and APT work. Complete reviews of FIM and APT are available elsewhere.^{40,41}

A number of examples exist that suggest organic specimens can be fabricated and remain sufficiently stable to allow APT analysis. The ultimate structural conclusions that can be drawn from the information content gathered via APT remains an active area of research.^{38,42}

All of the challenges identified in the previous section remain or are exacerbated when attempting to perform voltage-pulsed APT on electrically insulating materials. Before any data collection

can be attempted, prospective specimens must be fashioned either into the shape of a needle or as a thin coating at the apex of a sharp needle, while preserving adequate specimen conductivity to promote a minimally attenuated and broadened pulsed field at the apex.⁴³ Beginning in the mid-1980s, two groups (including one of the authors, Nishikawa) became the first to overcome these obstacles to investigate electrically conducting polypyrrole (PPy).^{30,31} Specimens were prepared by electrochemically depositing thin films onto sharp platinum tips. Since many biomolecules are simply biopolymers, they share many similar structural and compositional traits with organic polymers. Organic polymers have chemical structures that are comparatively simple and

well known and are therefore reconcilable with the observed mass spectra. Validation of APT applicability to biomaterials is therefore more readily accomplished by successful analysis of organic polymers. Conducting polymers have desirable electrical transport characteristics that aid the field evaporation process and alleviate potential concerns related to electrical conductivity for a proof-of-principle investigation.

Both investigations utilized similar 1D atom probe instrumentation that allowed for the analysis of approximately 1 to 2-nm diameter regions of the specimen surface at a depth rate of ~ 100 ion nm^{-1} .³¹ The narrow field-of-view of these instruments allowed only for mass analysis without imaging; however, parallel large field-of-view (100 nm^2) FIM capability of the instrument allowed for observation of the surface structure when the specimens remained viable at the fields necessary to perform FIM. Even though these polymer films were grown using very similar techniques, differences in the polymer microstructure are always possible.⁴⁴ Besides real differences in microstructure, other differences in mass spectra would be expected based on differences in analysis/instrumentation conditions such as specimen temperature, pulse fraction, and peak shape, which all can affect ion distributions as observed in other analyses.⁴⁰

For PPy ($(\text{NC}_4\text{H}_3)_n$), Maruyama et al. observed mass peaks at 65, 140, and 210 Da and identified them as singly charged PPy monomers, dimers, and trimers.³⁰ Conversely, Nishikawa and Kato did not observe PPy field evaporating as complete molecular fragments.³¹ They found that both ClO_4 -doped and BF_4 -doped polymers exhibited mass peaks dominated by singly and doubly charged carbon-, nitrogen-, and oxygen-containing fragments—CO, COH, CNH, CNO, CO_2 , CO_2H , and C_2H_2 . Hydrogen FIM of these tips revealed disordered, distributed bright spots that evolved in an orderly fashion during field evaporation, indicative of the disordered structure of PPy but also suggestive of a stable specimen structure under high field. Although each investigation resulted in a different mass fingerprint for PPy field-evaporation, together they demonstrated that polymers could be electrochemically deposited on ~ 100 -nm sharp metal carrier tips and successfully mass analyzed.

In time-of-flight mass spectrometry of inorganics, where most ions are monatomic, most peaks in the spectrum can be uniquely identified or decomposed into constituents. With organic materials, most ions are polyatomic. This fact greatly

increases the complexity of peak identification. Ambiguities in peak identification are a common occurrence for organic materials and are one of the challenges for the technique.

Since these initial studies, little APT of organic materials had been reported in the literature, until recently.³⁰⁻³⁹ PLAP of biomolecules has invited renewed evaluation because pulsed-laser evaporation diminishes the electrical conductivity requirement⁴⁰ for the specimen. Unlike pulsed-voltage evaporation, which has been under active study for more than 40 years and whose properties are well established,^{40,43} PLAP introduces a set of new analysis conditions, whose effects on field evaporation are still subject to some debate. The laser pulse briefly raises the specimen apex temperature (by about 100 K), which lowers the electrical field required to create ions, and so characteristics of the laser pulse (duration, wavelength, spot size) influence the analysis and require investigation.^{36,45-47} Since organic molecules typically have structural phase transitions at temperatures far below those of the inorganic materials typically analyzed with PLAP, understanding the influence of these characteristics is especially important here.

The challenge for APT applied to any discipline has always been how to fashion a material of interest into the form of a ~ 100 nm sharp needle. Because specimen preparation is the first step for any analysis by APT, it is worthwhile to review the techniques appropriate for biomaterials.

Specimen Preparation is the Key

The most important step in microscopy, though often the least glamorous, is preparation of a high-quality specimen. APT is no exception. You may see that the applications that follow have all worked around the specimen preparation challenge, but none has achieved a general solution for organic and biological materials. Most of the effort and complication in specimen preparation today is due to a lack of developed techniques and hardware for the purpose. The situation is, however, almost directly analogous to preparation of specimens for TEM, and efforts are under way to adapt these technologies directly for APT.

Two basic approaches to preparation of organic specimens for APT must be recognized: (1) a thin coating is applied to a pre-formed needle of the right size; or (2) a monolithic material is prepared into an appropriate needle-shaped specimen. Furthermore, a crucial distinction must be made between specimen preparation at room temperature and specimen prepara-

tion at cryogenic temperatures (~ 77 K). The latter makes it possible to consider virtually any organic material, but it requires the most technique and hardware development.

Organic materials typically must be stabilized against deformation and vaporization during preparation and subsequent analysis in vacuum. They also must be protected from environmental degradation, such as frost buildup, during handling. Chemical stabilization using cross-linking agents, such as osmium, can be effective, but it also may alter the structure of the specimen and is therefore undesirable. Cooling the specimen accomplishes stabilizations with little or no alteration of the structure, so cryogenic specimen preparation is the most general path forward for certain specimen types.⁴⁸ This seems especially true for site-specific specimen preparation of biological materials.

Polymeric or other organic coatings on a carrier needle must adhere adequately to the surface if they are to withstand the high stresses in APT. Coating layers must be thick (~ 5 nm or greater) to ensure that the data recorded can be distinguished from thin contamination layers on the carrier needle.

Since polymer films or multi-component epoxies are cured at room temperature, polymers are a logical choice to use as room-temperature embedments for biomolecules; however, the mass spectrum from a polymeric embedment can be complex, as illustrated in Figure 2. Frozen water as an embedment is desirable because it has a simple, well-understood mass spectrum,^{49,50} and it is known and trusted in the life-science community as an embedding material.

Cryofixation is a well-established group of techniques that includes plunge freezing, high-pressure freezing, and slam freezing. All of the requirements for cryopreparation and cryo-transfer have been mastered independently for many biological materials for TEM analysis.⁴⁸ In TEM, frozen specimens are often created in a geometry directly suitable for analysis. All that is required is careful transfer of the specimen from the cryofixation environment into the microscope without contamination by frost, while maintaining a suitable temperature. These techniques must and will be adapted to APT, and while some success has been achieved in this regard,⁵¹ no general cryofixation method has been identified that allows for the cryofixation of APT specimens in a geometry that is suitable for analysis. Consequently, a number of additional cryo-transfer steps are likely required to

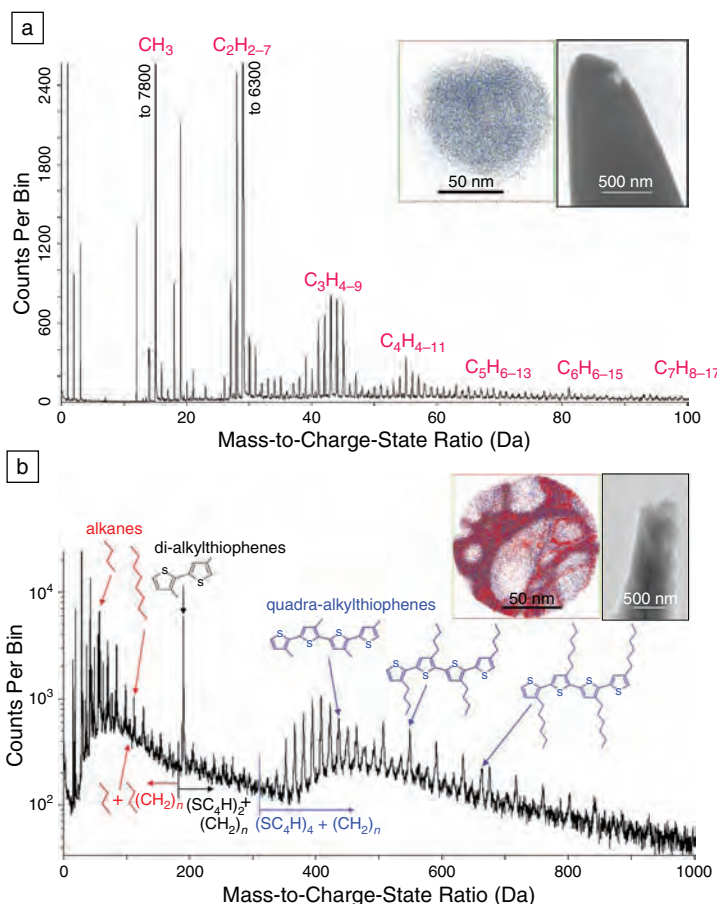


Figure 2. Mass spectrum for poly(3-dodecylthiophene). These materials field evaporate in a reproducible manner, although the details of the mass spectrum may not be fully understood. (a) Dip-deposition. Coating and evaporation are uniform, as evident both by scanning electron microscopy (inset top right) and by the three-dimensional image that shows the spatial distribution of events at the detector when viewed down the analysis direction (inset top left). Blue dots represent CH_n molecular ions; black dots represent C_2H_n molecular ions; and gray dots represent C_3H_n molecular ions. (b) Electro spray deposition. Many large peaks are observed, and an extremely nonuniform deposition is evident by scanning electron microscopy (inset top right). Spatial distributions of small fragments (alkanes) and large fragments (quadra-alkylthiophenes) are displayed as red and blue dots, respectively (inset top left). Used with permission from Reference 35.

facilitate the specimen transfer among the various instruments required for specimen shaping and characterization (i.e., plunge freezing with cryo-transfer to a cryo-focused ion beam (FIB) microscope for specimen shaping, cryo-transfer to a cryo-TEM to pre-screen and characterize prospective APT specimens, and cryo-transfer to a cryo-APT for analysis). Rapid freezing techniques that form vitreous water ice in surface layers greater than about 100-nm thick may be directly adapted from existing methods used for TEM preparation. The success of FIB lift-out for site-specific specimen preparation of inorganic materials makes cryo-FIB lift-out a logical choice for site-specific speci-

men preparation of biological materials; however, the general cryo-FIB lift-out technique requires significant development, but recent progress in cryo-FIB for TEM preparation is encouraging.⁵²

Local-electrode geometries have opened up a host of strategies that require protrusions on the order of 10 to 100 micrometers in height. One novel instrument developed by Nishikawa, the scanning atom probe (SAP), utilizes a local electrode coupled with an extended tip, allowing for pre-APT scanning tunneling microscopy (STM) and atomic force microscopy (AFM) measurements to discover protrusions suitable for subsequent analysis.⁵³⁻⁵⁵ Two successful specimen preparation strategies

used by the SAP include (1) taking a thin polymer film, peeling it from a substrate using tweezers, and analyzing protrusions as they exist on the edges; and (2) tacking small clumps of tangled nanowires with epoxy and analyzing individual nanowires.³² Another proposed strategy, compatible with a local electrode, suggests forming molds of polymer microtips (100 micrometer tall micro-needles), which might allow for analysis of the polymer itself or organic molecules embedded within the microtip-shaped polymer matrix.⁵⁶ Finally, strategies incorporating lift-out specimen preparation originally developed for TEM allow for analysis of specimens originally deposited onto flat substrates.⁵⁷ These specimens are typically lifted out and attached to microtips, enabling an economical utilization of preparation time, though macroscopic needles also may be used.

Survey of APT Mass Analysis Results

This section surveys the most fully developed analyses to date performed on organic materials using APT.

Poly(3-alkylthiophene)s

Poly(3-alkylthiophene)s (P3ATs) contain a polythiophene backbone, making them conducting polymers with alkane side chains attached to every thiophene ring, rendering these materials soluble in a host of organic solvents and enhancing their processibility.⁴⁴ These two constituent types were analyzed separately: polythiophene⁴⁴ at room temperature with a 1D SAP,³² and alkane segments with both laser- and voltage-pulsing modes at cryogenic temperatures on a commercial 3D local-electrode atom probe (LEAP).³³ Multiple specimens consisting of the P3AT varieties most commonly studied and considered for electronic devices, poly(3-hexylthiophene), poly(3-octylthiophene), and poly(3-dodecylthiophene), were deposited onto sharp aluminum carriers, analyzed using a LEAP tomograph under a variety of analysis conditions, and prepared via dip-deposition and electro spray ionization (ESI)-deposition techniques.^{34,39}

Dip-deposited films exhibited only low-mass alkane fragments with no mass peaks beyond ~100 Da, Figure 2. By making a rudimentary set of chemical assignments for sulfur- and carbon-containing mass peaks, subtle variations in relative peak intensities were shown to match roughly the underlying stoichiometry of the different polymers. Ion images for these films revealed extremely uniform distributions of all ion fragments compatible

with the smooth film surfaces seen in scanning electron microscopy (SEM) images of the same tips, Figure 2. Many tips without deposits were analyzed and exhibited mass spectra from surface contamination that strongly resembled that of the dip-deposited films. The strongest peaks in the polymer mass spectra, 29, 15, 28, and 44 Da, respectively, were often observed with similar relative intensities during the first 1–2 nm of material removed from clean carrier tips. Therefore, care was taken to distinguish possible surface contamination from the bulk of the polymer in all cases.

ESI-deposited films exhibited unique mass fingerprints dependent on the side chain length. Essentially, three types of fragments were identified, Figure 2b: (1) alkane fragments with variable hydrogen content were the most intense peaks in the 15 to 100 Da range (similar to dip-deposited specimens mentioned previously); (2) quadra-thiophene peaks with variable alkane content prevalent in the >300 Da range had a relative intensity that was repeatably dependent on P3AT type; and (3) the appearance of di-thiophene fragments at >190 Da, which were only observed after exposure to high laser-pulse energies, were indicative of subtle structural changes induced by this thermal history. Ion images of the tip surface (red and blue inset, Figure 2b) reflect the rough topology of the tip surface also observed in the SEM image of the same tip (gray scale inset, Figure 2b).

The feasibility of P3ATs as a matrix for embedding other molecules of interest was also considered. Because P3ATs can be doped with C_{60} , making them conductive, and because both are soluble in the same solvents, dip-co-deposited films were prepared.^{35,36} These deposits exhibit the same mass spectra as those reported for undoped dip-deposited films mentioned earlier.^{35,36} New peaks at 720 and 360 Da (and elsewhere) were identified as C_{60}^+ and C_{60}^{2+} , respectively. At elevated laser pulse energies, no intact C_{60} molecules were observed but were replaced by intensified C_{10}^+ and C_{18}^+ ion fragment peaks. Ion imaging revealed phase-separated regions rich in P3AT and C_{60} reminiscent of a morphology common in many polymer-blended structures.

An ideal embedding matrix for APT would provide minimal overlap of ion mass fragments with those originating from embedded molecules in order to avoid additional ambiguities in the chemical identifications. P3ATs generally do not fulfill this requirement because a large number of mass peaks are observed during analysis, except in the case where the

embedded molecules occupy a unique region of the mass spectrum as C_{60} molecules do when the laser-pulse energy is sufficiently low. This study also suggests that ion fragments, from both the matrix and the embedded molecules, might be manipulated by an appropriate choice of laser-pulse energy that minimizes any overlaps in the mass spectrum.

Self-Assembled Monolayers

Self-assembled monolayers (SAMs) can be considered both as surface-modifying agents, enabling more advanced specimen preparation strategies for APT, and as a class of materials. These materials happen to be self-assembled structures but also serve as a way to chemically control surfaces. Thus, this single demonstration overlaps two classes of materials and represents structures and surfaces approximating those found in biology, such as cell membranes and surfaces. Results of SAM deposits on field-formed metal tips have been reported for both pulsed-voltage³⁸ and pulsed-laser modes.³⁹ Independent of the field-evaporation method, each shows an evolution of alkane ion fragments up to the sulfur-metal interface, similar to those for octadecanethiol bulk and P3AT deposits described previously. These measurements demonstrate typical APT imaging capability, revealing a uniform structure parallel to the surface and expected composition variation and interfacial information normal to the surface.

Amino Acids

APT mass analysis of amino acids has been attempted by depositing molecules among clumps of single-walled carbon

nanotubes (SWCNTs),⁵⁸ grown by the high-pressure carbon mono-oxide process (HiPCO).⁵⁹ Densely packed SWCNT fibers enable production of specimens with ample quantities of biomolecules drawn in via capillary action that avoid catalytic modification due to contact with a metal carrier. A ball of tangled long SWCNT fibers, several tens of micrometers in diameter, was silver pasted onto a tungsten tip and then dipped in a solution of sample molecules of glycine, cysteine, leucine, or methionine.⁶⁰

These amino acids were chosen because of their relative chemical simplicity: glycine was specifically chosen because it is the smallest amino acid and hopefully produced a simple and predictable mass spectrum; leucine is structurally similar with the addition of a hydrocarbon side chain; methionine and cysteine are sulfur containing. It was hoped that the analysis of these amino acids would provide a guideline for the analysis of larger molecules. It was also expected that glycine molecules would be dissociated into its major groups. However, the mass spectrum obtained from glycine was not as simple as hoped because of mass overlaps, such as C_3^{2+} and H_2O^+ , Figure 3.⁵⁹

Applications Prospects

While the spectrum of applications will continue to evolve, a few examples of how APT may be used to study biological materials are listed. In many cases, bioscientists or polymer scientists know the global structure and nominal composition of biological materials or polymers, respectively. The challenges involve learning about small-scale structures, such as that which occur at internal interfaces.

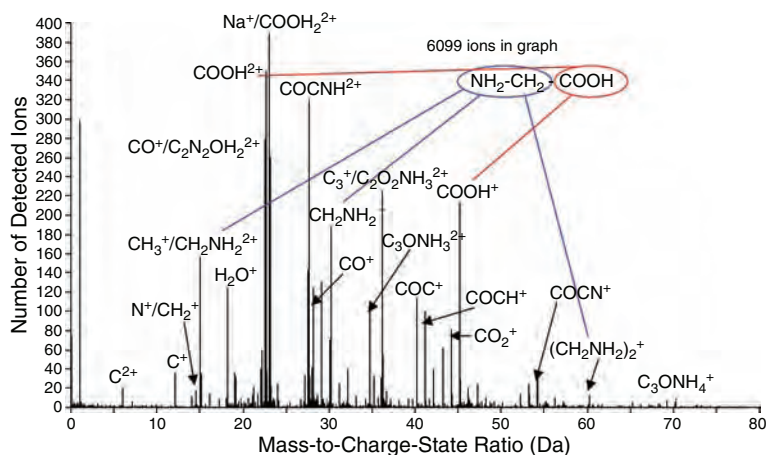


Figure 3. Mass spectrum from glycine on single-walled carbon nanotubes obtained in a scanning atom probe. Used with permission from Reference 60.

These examples might include a phase boundary in a block copolymer, the surface of an inorganic nanoparticle functionalized for use in medicine, the growth patterns in biomineral composites such as bone or seashell, or the layers of organic light-emitting diodes. Indeed, the exact composition and structure of many biological structures such as the intracellular matrix at the subnanometer scale are likely to hold many important surprises. How does this differ between healthy cells and cancerous cells? One thing is almost always true in microscopy: ignorance is bliss, and knowledge is an opportunity.

An extreme example for APT application to organics would make use of the 3D positioning of the molecular ions to determine structural information about biomolecules. For example, the conformation of a protein molecule in ice might, in principle, be determined from very small volumes (zeptoliters) of molecules in solution. This could obviate the need for crystallization and might enable conformation determination for membrane proteins. It would also open up the prospect of analyzing proteins in their natural environment with or without small molecule drugs attached. These are lofty goals that may not be readily achievable, but they are nonetheless suggested by comparable success with inorganic materials. Significant developments in techniques and instrumentation will, however, need to occur first.

Summary

Atom-probe tomography (APT) on organic materials is far more complex than for inorganic materials. Its practical value has yet to be fully demonstrated. Reproducible mass spectra have been obtained on synthetic polymers but not yet on organic biological materials.

Continued advances in specimen preparation remains key to realizing real applications. Avenues for room-temperature specimen preparation will continue to be an active area of research with the development of strategies such as polymer embedding showing some promise, but complications arising from mass spectrum overlaps and complexity may limit its general application. Development of cryo-prep methods may eliminate most of the mass spectrum overlap issues, but much work remains to be done in order to transfer developed methodology from electron microscopy to APT. Ultimately, the prospects and timeline for investigating nanobiology with APT may depend on developing methods that enable cryo-FIB lift-out for site-specific specimen prepara-

tion of biological materials embedded within a frozen water matrix.

Acknowledgments

The authors would like to acknowledge much of the prior work performed at Imago by Steven Goodman and Stephanie Kostna-Keeney. Funding for much of that work was provided by the National Science Foundation under grant #0216620. Support from the U.S. Defense Advanced Research Projects Agency for TFK and TJP is also gratefully acknowledged.

References

1. E.W. Müller, *Naturwissenschaften* **14**, 333 (1950).
2. E.W. Müller, *Naturf* **5**, 475 (1950).
3. E.W. Müller, *Ergeb. Exakten Naturwiss.* **27**, 290 (1953).
4. A.J. Melmed, E.W. Müller, *J. Chem. Phys.* **29**, 1037 (1958).
5. E.W. Müller, *LIFE* **28**, 67 (1950).
6. E.W. Müller, *Sci. Am.* **186**, 58 (1952).
7. P. Wolf, *Z. Angew. Phys.* **6**, 529 (1954).
8. E. Horl, F. Strangler, *Acta Phys. Austriaca* **10**, 1 (1956).
9. J.A. Becker, R.G. Brandes, *J. Appl. Phys.* **27**, 221 (1956).
10. A.P. Komar, A.A. Komar, *Sov. Phys. Tech. Phys.* **6**, 166 (1972).
11. I. Giaever, *Surf. Sci.* **29**, 1 (1972).
12. G.R. Condon, J.A. Panitz, *J. Vac. Sci. Technol., B* **18**, 1216 (2000).
13. E.W. Müller, *Z. Naturf.* **11a**, 88 (1956).
14. E.W. Müller, *J. Appl. Phys.* **27**, 474 (1956).
15. R.C. Abbott, *Rev. Sci. Instrum.* **36**, 1233 (1965).
16. T. Gurney, F. Hutchinson, R. Young, *J. Chem. Phys.* **42**, 3939 (1965).
17. E.W. Müller, K.D. Rendulic, *Science* **156**, 961 (1967).
18. W.R. Graham, F. Hutchinson, D.A. Reed, *J. Appl. Phys.* **44**, 5155 (1973).
19. E.S. Machlin, A. Freilich, D.C. Agrawal, J.J. Burton, C.L. Briant, *J. Microsc.* **104**, 127 (1975).
20. J.A. Panitz, I. Giaver, *Ultramicroscopy* **6**, 3 (1981).
21. J.A. Panitz, C.L. Andrews, D.G. Bear, *J. Electron. Microsc. Technol.* **2**, 285 (1985).
22. J.A. Panitz, *Rev. Sci. Instrum.* **56**, 572 (September 4, 1984, 1985).
23. J.A. Panitz, *Proceedings of the 39th Annual Meeting of the Electron Microscope Society* **18** (1981).
24. J.A. Panitz, *J. Microsc.* **125**, 3 (1982).
25. J.A. Pantiz, J. Ghiglia, *J. Microsc.* **127**, 259 (1982).
26. J.A. Panitz, *Ultramicroscopy* **7**, 241 (1982).
27. J.A. Panitz, *Ultramicroscopy* **11**, 161 (1983).
28. J.A. Panitz, *The Analysis of Organic and Biological Surfaces*. P. Echlin, Ed., (Wiley, New York, 1984), p. 171.
29. J.A. Panitz, *Microsc. Microanal.* **11** (Suppl. 2), 92 (2005).
30. T. Maruyama, Y. Hasegawa, T. Nishi, T. Sakurai, *J. Phys. Colloq.* **C6**, 6 (1987).
31. O. Nishikawa, H. Kato, *J. Chem. Phys.* **85**, 6758 (1986).

32. O. Nishikawa, M. Taniguchi, *Chin. J. Phys.* **43**, 111 (February 2005).
33. T.J. Prosa, S. Kostna Keeney, T.F. Kelly, *Microsc. Microanal.* **15** (2009).
34. T.J. Prosa, S. Kostna Keeney, T.F. Kelly, *J. Microsc.* (2009), (in press).
35. T.J. Prosa, S. Kostna Keeney, T.F. Kelly, *Microsc. Microanal.* **13**, 190 (2007).
36. T.J. Prosa, R.A. Alvis, T.F. Kelly, *Microsc. Microanal.* **14**, 1236 (2008).
37. O. Nishikawa, M. Taniguchi, S. Watanabe, A. Yamagishi, T. Sasaki, *Jpn. J. Appl. Phys.* **45**, 1892 (July 3, 2005, 2006).
38. B. Gault, W. Yang, R.K. Zheng, F. Braet, S.P. Ringer, *Microsc. Microanal.* **15** (2009).
39. T.J. Prosa, S.L.P. Kostna, T.F. Kelly, *50th International Field Emission Symposium* **533** (2006).
40. M.K. Miller, *Atom Probe Tomography: Analysis at the Atomic Level* (Kluwer Academic/Plenum Publishers, New York, 2000).
41. T.F. Kelly, M.K. Miller, *Rev. Sci. Instrum.* **78**, 031101 (2007).
42. F. Braet, L. Soon, T.F. Kelly, D.J. Larson, S.P. Ringer, in *Nanotechnologies for the Life Sciences* (Wiley-VCH, 2006), vol. 3, pp. 292–318.
43. M.K. Miller, A. Cerezo, M.G. Hetherington, G.D.W. Smith, *Atom Probe Field Ion Microscopy* (Oxford University Press, Oxford, 1996).
44. T.A. Skotheim, R.L. Elsenbaumer, J.R. Reynolds, Eds., *Handbook of Conducting Polymers* (Merrel Dekker, New York, 1998).
45. J.H. Bunton, J.D. Olson, D.R. Lenz, T.F. Kelly, *Microsc. Microanal.* **13**, 418 (2007).
46. T.T. Tsong, *Atom-Probe Field Ion Microscopy: Field Ion Emission and Surfaces and Interfaces at Atomic Resolution* (Cambridge University Press, Cambridge, 1990).
47. B. Gault, A. Vella, F. Vurpillot, A. Menand, D. Blavette, B. Deconihout, *Ultramicroscopy* **107**, 713 (2007).
48. J.R. McIntosh, *Cellular Electron Microscopy Volume 79* (Academic Press, New York, 1987).
49. J.A. Panitz, *J. Vac. Sci. Technol., A* **7**, 2850 (1989).
50. J.A. Panitz, A. Stintz, *J. Vac. Sci. Technol., A* **9**, 1365 (1991).
51. J.A. Panitz, *Microsc. Microanal.* **14**(2), 122 (2008).
52. M. Marko, C. Hsieh, R. Schalek, J. Frank, C. Mannella, *Nat. Methods* **4**, 215 (2007).
53. O. Nishikawa, M. Kimoto, *Appl. Surf. Sci.* **76/77**, 424 (1994).
54. O. Nishikawa, M. Kimoto, M. Iwatsuki, Y. Ishikawa, *J. Vac. Sci. Technol., B* **13**, 599 (1995).
55. O. Nishikawa, Y. Ohtani, K. Maeda, M. Watanabe, K. Tanaka, *Mater. Charact.* **44**, 29 (2000).
56. S.L.P. Kostna, T.J. Mengelt, M. ALi, D.J. Larson, S.L. Goodman, T.F. Kelly, *Microsc. Microanal.* **11**, 874 (2005).
57. K. Thompson, D.J. Lawrence, D.J. Larson, J.D. Olson, T.F. Kelly, B. Gorman, *Ultramicroscopy* **107**, 131 (2007).
58. O. Nishikawa, M. Taniguchi, *J. Vac. Sci. Technol., A* **26**, 1074 (2008).
59. M.J. Bronikowski, P.A. Willis, D.T. Colbert, K.A. Smith, R.E. Smalley, *J. Vac. Sci. Technol., A* **19**, 1800 (2001).
60. O. Nishikawa, M. Taniguchi, A. Ikai, *Proceedings of the Nanotech Conference and Expo 2009*, Houston, TX, George Brown Convention Center, 2009. □

Preferential Growth of Metallic SWNTs Achieved

One obstacle to the implementation of single-walled carbon nanotubes (SWNTs) in electronic devices is that their synthesis results in a mixture of conducting and semiconducting species. Progress has been made in separating SWNTs based on their conductivities, which is determined by chirality. Some progress has been made in controlling SWNT structure during growth (e.g., semiconducting SWNTs are produced preferentially by plasma-enhanced chemical vapor deposition), demonstrating that somewhat different mechanisms lead to different chiralities. Recently, A.R. Harutyunyan and co-researchers at the Honda Research Institute, Columbus, Ohio, in collaboration with T.M. Paronyan of the University of Louisville, S.M. Kim of Purdue University, and their colleagues, were able to increase the fraction of CNTs with metallic conductivity grown from Fe nanocatalysts from 33% to a maximum of 91% by varying the conditions under which the catalyst was annealed.

As reported in the October 2 issue of *Science* (DOI: 10.1126/science.1177599;

p. 116), Harutyunyan and co-researchers annealed *in situ* Fe nanocatalysts deposited onto a flat SiO₂/Si support, using an ambient atmosphere of He or Ar, and varying ratios of H₂ and H₂O. Using methane as the carbon source, SWNT synthesis was performed at 860°C. The researchers observed with scanning electron microscopy that increasing the concentration of reductive species (Ar:H₂ was increased from 9:1 to 8:2 at 840 Torr with ~3.5 mTorr H₂O) during catalyst conditioning resulted in higher densities of SWNTs on the substrate. This led them to perform a systematic study of SWNT growth on catalysts annealed *in situ* under varying ambient conditions. The ratio of metallic to semiconducting tubes was obtained by measuring the SWNT's Raman breathing modes, specifically, $R = I_{\text{met}}/I_{\text{sem}}$ where I_{met} and I_{sem} are the integrated intensities of the metallic and semiconducting SWNTs, respectively. The researchers observed an increase in R by (1) replacing Ar with He; (2) increasing the H₂ content in the Ar-H₂ atmosphere; and (3) increasing the annealing time from 1 minute to 10 minutes. A very high R value of 20.2, which corresponds to over 90% metallic SWNTs, was

obtained with a He:H₂ ratio of 8:2 and an annealing duration of 10 minutes.

The researchers verified their Raman spectra analysis by measuring field-effect transistor performance for 47 individual SWNTs and characterizing them according to their source-drain current. Another set of experiments demonstrated that the catalyst annealed in the presence of H₂O in the ambient atmosphere together with He promotes the growth of metallic tubes whereas semiconducting tubes are favored by catalysts annealed with an ambient atmosphere of H₂O and Ar. The researchers also investigated the mechanism of tube formation with *in situ* transmission electron microscopy of the Fe nanocatalysts under varying gaseous environments in analogy with the SWNT-synthesis conditions. Differences in both morphology and coarsening behavior of the nanocatalyst were observed.

The researchers said that "these catalyst rearrangements demonstrate that there are correlations between catalyst morphology and resulting nanotube electronic structure and indicate that chiral-selective growth may be possible."

STEVEN TROHALAKI

Quasicrystalline Order Revealed in Nanoparticle Superlattices

Quasicrystals are a class of materials that show sharp diffraction peaks despite presenting forbidden symmetry operations in classical crystallography. D.V. Talapin and M.I. Bodnarchuk from the University of Chicago; E.V. Shevchenko from Argonne National Laboratory; and X. Ye, J. Chen, and C.B. Murray from the University of Pennsylvania, have reported in the October 15 issue of *Nature* (DOI: 10.1038/nature08439; p. 964) that different binary nanoparticle colloidal systems can self-assemble into 12-fold rotational quasicrystalline order. According to the researchers, the compositional flexibility demonstrated that quasicrystal ordering could be a relatively common phenomenon in nanocrystal solids, with suitable size ratios between particles.

The researchers obtained the quasicrystalline nanoparticle assemblies by evaporating relatively concentrated colloidal solutions of 13.4-nm Fe₂O₃ and 5.0-nm Au monodisperse nanoparticles capped with oleic acid and dodecanethiol molecules, respectively, in tetrachloroethylene at 50°C under reduced pressure (~3.2 kPa) on a carbon-coated transmission electron microscopy grid or a silicon nitride membrane tilted by 60° or 70°. The researchers used the surfactant molecules to introduce short-range steric repulsion that counterbalanced the van der Waals forces and prevented uncontrollable aggregation of nanocrystals in the colloidal solution. They observed that during this process the nanocrystals self-assembled in AlB₂- and CaB₆-type phases, and on the (3².4.3.4) Archimedean tiling structure, depending on the Fe₂O₃-to-Au nanoparticle ratio. This structure is formed by five planar polygons (three triangles and two squares) sharing a common vertex in such a way that they fill the plane with no overlaps and no gaps, depending on the Fe. The nomenclature of these structures lists in order the polygons that meet at each vertex using integers that correspond to the numbers of sides of the polygons. So, the (3².4.3.4) structure consists of two triangles sharing a common edge, surrounded by two squares at each side of the triangles, and filling the empty space by another triangle, all of them

sharing a common vertex. In proximity to the (3².4.3.4) phase in the binary phase diagram of these nanoparticles, the researchers observed reproducible formation of a type of binary superstructure without translational symmetry. They observed that these structures showed sharp electron diffraction patterns revealing dodecagonal rotational symmetry, a symmetry operation forbidden in periodic structures. The researchers identified these self-assembled nanoparticle superstructures as dodecagonal quasicrystals (DDQC), a phase that formed also from colloidal solutions containing 12.6-nm Fe₃O₄ and 4.7-nm Au nanocrystals, and 9-nm PbS and 3-nm Pd nanocrystals, with size ratios between particles of ~0.43.

The researchers said that the space-filling factor had a significant effect on the relative stabilities of binary nanoparticle phases, and the quasi-periodicity could be a result of maximizing the entropy of arrangement of square and triangular "tiles." They consider that the discontinuity in the entropy density corresponding to the DDQC state might provide a mechanism for locking the quasicrystalline state over a range of nanocrystal concentration ratios. The researchers think that these studies will provide insight into the formation of the quasicrystal phase in atomic systems, and can be used as a convenient platform for detailed investigation of quasicrystal properties.

JOAN J. CARVAJAL

Addendum

David N. Seidman and Krystyna Stiller, Guest Editors of the theme "A Renaissance in Atom-Probe Tomography" (*MRS Bulletin*, October 2009), note that in 1973, J.A. Panitz invented the 10-cm atom probe (discussed on p. 745)—now called the imaging atom probe—which is the progenitor of all atom-probe tomographs, citing the following references: J.A. Panitz, *Rev. Sci. Instrum.* **44**, 1034 (1973) and J.A. Panitz, "Field Desorption Spectrometer," U.S. Patent 3868507 (1975).